Soft Matter

Accepted Manuscript

ROYAL SOCIETY OF CHEMISTRY

www.rsc.org/softmatter

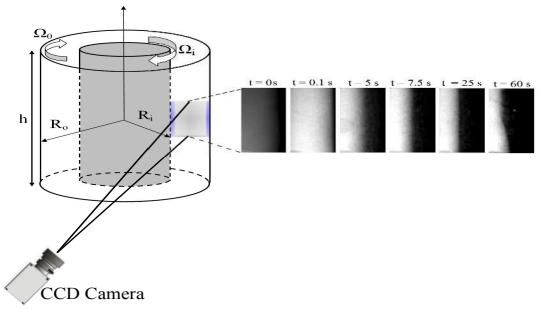

ARTICLE TYPE www. rsc.org/xxxxxx | XXXXXXXX

A flow visualization and superposition rheology study of shear-banding wormlike micelle solutions

Hadi Mohammadigoushki,[a] and Susan J. Muller*[a]

In this paper, we use rheometry and flow visualization to study the dynamics of the interface between shear bands in a wormlike micellar solution sheared between concentric cylinders, i.e., in a Taylor-Couette (TC) cell, and to evaluate the stress diffusion coefficient and the stress correlation length in the Johnson-Segalman model. Two wormlike micellar solutions are studied: an aqueous solution of CTAB-$NaNO_3$ and a solution of CPCl-NaSal in brine. These systems are highly elastic, exhibit Maxwellian behavior in linear viscoelasticity experiments, and shear banding in nonlinear experiments [Lerouge, S. *et al., Soft Matter*, 2008, **4**, 1808-1819, Fardin, M. A. *et al., Soft Matter*, 2012, **8**, 39,10072-10089, Ballesta, P. *et al., J. Rheol.*, 2007, **51**, 1047]. A large, custom-built, computer controlled TC cell allows us to rotate both cylinders independently and to visualize the flow in the r-z plane using a CCD camera. At low shear rates, the flow is stable and the fluid appears homogeneous throughout the gap between the cylinders. Above a critical shear rate, a shear banding transition occurs. This manifests itself in the formation of two distinct bands in the r-z plane, with an interface between the two bands. For sufficiently high ramp speeds, multiple step of interface evolution are identified, as noted by Radulescu, Lerouge, and others [Redulescu, O. *et al., Europhys. Lett.*, 2003. **62**, 230, Lerouge, S. *et al., Soft Matter*, 2008, **4**, 1808-1819]. We quantify the interface travel using direct visualization and use this measure, as well as superposition rheometry [Ballesta, P. *et al., J. Rheol.*, 2007, **51**, 1047], to determine the stress diffusion coefficient D and the stress correlation length ζ in the Johnson-Segalman model. These parameters are evaluated at different temperatures, shear rates, and gap sizes. We find that the stress diffusion coefficient and the stress correlation length exhibit a strong dependence on the gap of the Taylor-Couette cell for both shear-banding systems. For the CTAB-$NaNO_3$ system, we report a linear dependence of the stress diffusion coefficient on temperature for the parameter range considered. In addition, we find that for this system, the stress diffusion coefficient is independent of shear rate. For the CPCl-NaSal system, we observe the same color changes in the sample reported by others on extended light exposure; however, we find that different histories of light exposure do not affect the measured stress diffusion coefficient.

1 Introduction & Background

Complex fluids are found abundantly in nature, yet our understanding of them is far from complete. Most complex fluids exhibit unusual mechanical responses to the applied stress that are mainly due to the coupling of their microstructure and the flow field[1]. Therefore, any change in their internal structure can drastically alter the response of the fluid in different flow fields. Shear localization or shear banding is one example of a non-linear response of some complex fluids to flow. Under certain conditions, some complex fluids such as soft glassy materials, suspensions, granular materials or wormlike micelles exhibit shear banding[2–5]. When these fluids experience a shear rate that exceeds a critical value, the flow becomes inhomogeneous such that shear bands with different viscosities co-exist. These shear bands are separated along the gradient direction and have the same shear stress[6–8].

Among fluids that exhibit shear-banding, wormlike micellar solutions have received considerable attention in the last few decades and therefore, their dynamics in flow are well documented[6,8–11]. Wormlike micellar solutions are typically composed of a cationic surfactant and a counterion that are dissolved in water. These fluids are used in oil recovery applications, as drag reducing agents, and in personal care products. Given the right conditions of concentration and temperature, the surfactants aggregate into long, flexible cylindrical micelles that are entangled in the aqueous medium[12]. This complex fluid shares some similarities with polymer solutions. But, unlike polymer solutions, the wormlike chains can break and reform under flow. Hence, they have been described as living polymers[6,7,13]. Under shear-banding conditions, wormlike micelles tend to be elongated in the direction of flow in the high shear rate band. On the other hand, wormlike chains are randomly oriented and entangled in the low shear rate band[14–16].

[a]*Department of Chemical and Biomolecular Engineering, University of California, Berkeley, California 94720, United States*
**E-mail: muller2@berkeley.edu*

The rheology of different wormlike micellar systems has been studied both experimentally and theoretically. On the experimental side, the mechanical signature for shear banding in wormlike micelles was first provided by Rehage *et al.*[10]. They showed that in steady shear experiments at low shear rates, the shear stress increases monotonically with the shear rate ($\dot{\gamma} < \dot{\gamma}_l$), shows a stress plateau for a range of shear rates ($\dot{\gamma}_l < \dot{\gamma} < \dot{\gamma}_h$), and for high shear rates ($\dot{\gamma} > \dot{\gamma}_h$), the shear stress again increases monotonically with the shear rate. Moreover, local velocity measurements showed the presence of bands with different shear rates that coincided with the intermediate range of shear rates ($\dot{\gamma}_l < \dot{\gamma} < \dot{\gamma}_h$) from steady shear rheometry[17–19]. Under certain conditions of concentration and temperature wormlike micelles have been shown to primarily follow the single mode Maxwell viscoelastic model in linear viscoelasticity measurements[20]. Other experiments have examined the effect of concentration of constituents and temperature on the flow behavior of wormlike micelles[8,21–23].

On the theoretical side, there are a few theories suggested for this system that are based on different constitutive models. For instance, Cates developed a theory that couples the reptation theory of de Gennes and Doi and Edwards with reaction terms that account for scission and reformation of chains under flow[20]. Cates' theory predicts that if the time scale associated with the scission and reformation of chains is shorter than the reptation time, then the fluid is primarily a single mode Maxwellian fluid for low to moderate frequencies. The constitutive equation derived by Cates and co-workers predicts a non-monotonic flow curve that is consistent with the formation of shear bands. In addition, the Johnson-Segalman (JS)[24] model, which is a semi-empirical model, also has a non-monotonic flow curve and has been widely used by researchers to predict instabilities in the flow of wormlike micelles[25–27]. The original Johnson-Segalman (JS) model is a special case of the Oldroyd eight-constant equation; the Oldroyd eight-constant equation relates the stress in a fluid to the flow history using a purely continuum mechanical derivation and imposing the constraints of frame invariance and including terms that are at most linear in the stress and quadratic in the rate of strain tensor and the stress combined. An important simplified case of the Oldroyd eight-constant model is the upper-convected Maxwell model, which can also be derived from either a temporary network model for Gaussian chains or from modeling the polymer chains as two Brownian beads connected by a Hookean spring. The Johnson-Segalman model is obtained by replacing the upper-convected derivative in the upper-convected Maxwell model by the Gordon-Schowalter convected derivative. The Gordon-Schowalter derivative is a linear generalization of the upper and lower convected derivatives, which allows for non-affine motion of polymer strands with respect to the continuum. A slip parameter a represents the reduction in stress relative to affine motion; that is, the fractional stretch of the polymeric material with respect to the macroscopic deformation of the continuum. For $a < 1$, the JS model predicts a non-monotonic relationship between shear stress σ_{xy} and shear rate $\dot{\gamma}$: multiple shear rates are possible for a given stress. In a specific range of shear rates, the slope of the flow curve is negative ($d\sigma_{xy}/d\dot{\gamma} < 0$) which represents an unstable state. In this unstable state, fluid splits into two differently sheared bands with each shear band lying on a stable part of the flow curve (having a positive slope).

These two models have been successful in predicting several aspects of the flow of wormlike micelles, but fail to predict other aspects that are reported in experiments[13,28]. For instance, Cates' theory does not predict an overshoot in the stress in startup of shear flow, which is contrary to the experimental observations[28]. For the Johnson-Segalman model, the flow curve is history dependent. That is, the selection of the plateau stress corresponding to a shear-banded state is indeterminate: simulations of flow using the JS model in a range of geometries indicate that the stress may lie within a range of stresses but its selection is dependent on the flow history[29–31]. This history-dependence, however, is inconsistent with experiments on wormlike micellar solutions that indicate shear-banding occurs at a well-defined plateau stress that is history-independent[32–35].

As demonstrated by Olmsted *et al.*[28], adding a stress diffusion gradient term to the Johnson-Segalman model resolves the history dependency of the JS model and provides a mechanism for the selection of the plateau stress. As a result, the diffusive Johnson-Segalman (dJS) model, containing a stress diffusion coefficient D, is widely used to model wormlike micellar solutions. A primary concern of the present work is measuring this stress diffusion coefficient; the form of the stress diffusion term is given in equation (3) below. For a stress tensor T, the momentum balance reads:

$$\rho(\partial_t + v \cdot \nabla)v = \nabla \cdot T \tag{1}$$

Where, ρ, v, and T are fluid density, velocity and total stress tensor respectively. The stress tensor is a combination of the (Newtonian) solvent stress and the polymer stress which can be written:

$$T = -pI + 2\eta A + \Sigma \tag{2}$$

Where, p, η, A, and Σ are pressure, solvent viscosity, the symmetric part of the velocity gradient tensor, and polymer stress respectively. In the diffusive Johnson-Segalman model, the polymer stress is given by:

$$(\partial_t + v\cdot\nabla)\,\Sigma + (\Omega\cdot\Sigma - \Sigma\cdot\Omega) - a(A\cdot\Sigma + \Sigma\cdot A) \;=\; 2\frac{\mu A}{\tau_R} - \frac{\Sigma}{\tau_R} + D\,\nabla^2\Sigma \tag{3}$$

Where, μ is the shear viscosity of wormlike micelles, D is the stress diffusion coefficient, τ_R is the Maxwellian relaxation time, a is the slip parameter, and Ω is the anti-symmetric part of the velocity gradient tensor. One can also define a stress correlation length, $\zeta = \sqrt{D\tau_R}$, which controls the interface thickness between shear bands.

The dJS model has been used recently to study the formation of shear bands and the hydrodynamic stability of a range of shear banding flows[15,25,26,28,36]. Experiments on wormlike micelles in the Taylor-Couette geometry revealed the formation of two bands above a critical shear rate and, more importantly, that the interface between bands undergoes a series of transitions and eventually becomes undulated[21,22,36–38]. This result was also produced by a linear stability analysis of a diffusive Johnson-Segalman fluid in Couette flow between parallel plates as well as in the cylindrical Taylor-Couette geometry[25,27]. In experiments, researchers have studied the effects of several parameters such as shear rate, temperature, concentration of components, and curvature of the Couette geometry on this instability[21]. Moreover, startup of steady shear experiments have shown very interesting dynamics for the transient shear stress within the shear banding regime. For instance, Radulescu *et al.*[15] demonstrated that upon a step in shear rate within the shear banding regime, the transient shear stress shows first a rapid overshoot on a time scale of about $0.1\tau_R$, followed by an undershoot with a time scale of $10\tau_R$, which is in turn followed by a very gradual stress relaxation towards a steady value that takes place over a time scale of $100\tau_R$. Numerical simulations indicated that these dynamics were associated with three stages: band destabilization (as the initial shear bands attempt to adjust to the change in shear rate), interface reconstruction, and interface travel towards its final equilibrium position. The interface travel stage is controlled by the stress diffusion coefficient[15].

Lerouge *et al.*[36] conducted similar experiments on wormlike micellar solutions and measured the transient shear stress for a step from $\dot{\gamma} = 0$ to a shear rate within the shear banding regime. They reported four different stages of stress evolution in their experiments. The first two were similar to the first two regimes reported by Radulescu *et al.*[15], however Lerouge *et al.*[36] reported a subsequent linear increase in shear stress followed by a mono-exponential increase in shear stress to its final value. Lerouge *et al.*[36] also directly visualized the gap between the co-axial cylinders in Taylor-Couette flow during the transient stress measurements. The changes in stress were attributed to the dynamics of the interface formation and evolution as follows. The first stage corresponds to formation of a high shear band that occupies the entire gap, and (as in the initial stage of the step experiments within the shear banding regime where an interface exists initially but undergoes destruction following the step), is accompanied by a rapid stress overshoot. As time progresses, the interface between the high shear band and low shear band forms, which corresponds to Radulescu *et al.*'s interface reconstruction stage. Interface reconstruction is associated with the quick reduction of the shear stress. Once the interface between these phases sharpens and is clearly visible, the interface travels towards the inner cylinder to reach its equilibrium radial position. This stage is associated with the linear increase in shear stress. Finally, Lerouge *et al.*[36] showed that after the interface travel stage, the interface becomes destabilized and changes its shape from a flat to an undulated interface. The mono-exponential stress increase at long times was attributed to the undulation of the interface during this fourth stage.

Among these stages and time scales, the third one is of interest in this paper (i.e., interface travel). As noted by Olmsted *et al.*[28], the interface travel stage is characterized by the stress diffusion coefficient in the diffusive Johnson-Segalman model. To the best of our knowledge the stress diffusion coefficient has been evaluated by three methods. First, the interface position can be tracked during interface travel, and the diffusion coefficient can be extracted from the trajectory of the interface[36]. Second, superposition rheology is an alternative method to determine the velocity of the interface during interface travel and hence, the diffusion coefficient[39]. Superposition rheology is a method by which a small amplitude oscillatory shear is added to a steady shear flow[40]. This method was introduced by Booij to study the dynamical behavior of polymer solutions far from equilibrium and was adapted by Ballesta *et al.*[39] to the study of wormlike micelles. Ballesta *et al.* developed a phenomenological model that allowed them to extract the velocity of the interface during the interface travel stage for a CPCl-NaSal wormlike micellar system[39]. Finally, microfluidics experiments have also been performed to determine the stress diffusion coefficient for sheared wormlike micellar fluids[41,42]. Masselon *et al.*[41] used particle image velocimetry to measure velocity profiles in microchannels and fit the velocity profiles using a constitutive equation involving a stress diffusion term.

A closer look at the values reported for stress diffusion coefficients and the corresponding stress correlation lengths reveals that there are significant discrepancies between the values obtained by the above methods. For instance, Radulescu *et al.*[15], reported the diffusion coefficient and the stress correlation length for the system of CTAB-$NaNO_3$ (0.3 M, 0.4 M) at T = 30 C, as $6.1\times10^{-14} m^2/s$, and 100 *nm*, whereas, Lerouge *et al.*[36] have estimated these parameters as about $7.1\times10^{-11} m^2/s$ and 4 μm for

the same system and the same temperature. Masselon *et al.*[41,42] showed that the stress correlation length for CTAB-$NaNO_3$ in confined microchannels is on the order of $3-8\ \mu m$ at T = 25 C. Masselon *et al.*[41,42] and Lerouge *et al.*[36,43] reported that for the CTAB-$NaNO_3$ system the stress correlation length is much larger than the mesh size of wormlike micelles (i.e. $\zeta \gg \xi$), where, the mesh size ξ can be estimated as $\xi \approx (k_B T/G_0)^{1/3}$. However, Radulescu *et al.*[15] concluded that for this system of wormlike micelles, $\zeta \approx \xi$. The inconsistencies in these results have been attributed to the fact that in Radulescu *et al.*[15] the longest stress relaxation time scale was mistakenly attributed to the interface travel stage while it is now known to be related to the nucleation of instability[36]. While superposition rheology has proven to be a useful method in determining the stress diffusion coefficient of the CPCl-NaSal system, unfortunately, there is no report for the CTAB-$NaNO_3$ system by this method. Meanwhile, there is no accepted microscopic theory for stress diffusion in systems of wormlike micelles that enables us to evaluate the experimental data. In addition, the effects of other parameters such as temperature and the effect of gap size on the stress diffusion coefficient and the stress correlation length have not been systematically studied before.

The primary goal of the present work is to measure the stress diffusion coefficient and the corresponding stress correlation length of the wormlike micellar solution CTAB-$NaNO_3$ more systematically at different temperatures, shear rates, and gap sizes. To the best of our knowledge, the effects of temperature and gap size on the stress diffusion coefficient of the CTAB-$NaNO_3$ system have never been reported in the literature. Regarding the effect of shear rate, Fardin *et al.*[43] indicate that for CTAB-$NaNO_3$, the stress diffusion coefficient varies non-monotonically with shear rate, with the data displaying significant scatter, whereas, for other systems like CPCl-NaSal the stress diffusion coefficient monotonically increases with shear rate. Our objective here is to revisit measurements of the stress diffusion coefficient for CTAB-$NaNO_3$ and to systematically vary the parameters noted above. Finally, we validate our methodology, and the effects of gap, by considering a second, well studied shear banding system of CPCl-NaSal in brine. The interface dynamics of this latter shear banding system have been shown to be sensitive to light exposure[22], although the bulk rheological properties are not. The hydrophilic head in the CPCl molecule is a pyridinium ring, which, in aqueous solution, is susceptible to opening by UV radiation. According to Fardin *et al.*[22], when exposed to light, cleavage of the pyridine ring produces aldehyde enamine, which further degrades by thermally activated processes. Fardin *et al.*[22] showed that this process is irreversible. Thus, the properties of the CPCl surfactant solution as well as its shear banding behavior may be affected by this process. Here, we consider the effect of light exposure on the stress diffusion coefficient for CPCl-NaSal. We perform measurements in two different ways. First, we perform startup of steady shear experiments in a large custom made Taylor-Couette cell to allow highly resolved visualization of the interface dynamics. Second, we conduct superposition rheology measurements in a commercial rheometer.

2 Experiments

2.1 Materials

The wormlike micellar solutions studied in this work are an aqueous solution of cetyltrimethylammonium bromide (CTAB) and sodium nitrate ($NaNO_3$) (both supplied by Fischer Scientific), and cetylpyridinium chloride (CPCl), and sodium salicylate (NaSal) in brine (Supplied by Spectrum Chemical and Fischer Scientific). We prepared solutions of 0.3 M CTAB and 0.4 M $NaNO_3$ in water and 8% wt of CPCl in brine (0.5 M NaCl) with the molar ratio of [NaSal]/[CPCl] = 0.5 with a magnetic stirrer and left them at room temperature for a few days before doing experiments. For experiments in the Taylor-Couette cell we added a small amount of mica flakes (0.001wt%) to visualize the flow field. This small amount does not affect the rheology of the solution. Mica flakes are anisotropic particles that orient in the direction of flow, which in turn enables us to visualize the flow field. Although the density of mica flakes is about 3.0 g/cm^3 and the fluid density is about 1.1 g/cm^3, they settle very slowly (on the order of weeks) due to their small size and the high viscosity of the fluid.

2.2 Methods

Experiments are carried out in two different setups: a commercial rheometer and a large, custom-built Taylor-Couette (TC) cell. We use a Malvern-Gemini stress controlled rheometer to characterize the rheology of wormlike micelles at different temperatures by doing both linear and non-linear viscoelastic tests. The linear and non-linear tests are carried out in both a cone-and-plate geometry and in a Couette co-axial cylinders geometry with R_i = 12.5 mm and R_o = 13.75 mm, where R_i and R_o are the inner and outer cylinder radii. We also use the rheometer to carry out superposition rheology experiments in which a small amplitude oscillatory shear is superimposed on steady shear. The superposition rheology experiments are carried out in three different Mooney-Couette (co-axial cylinders with conical bottoms) geometries with different gap sizes, d = 1.25 mm, d = 0.75 mm, and d

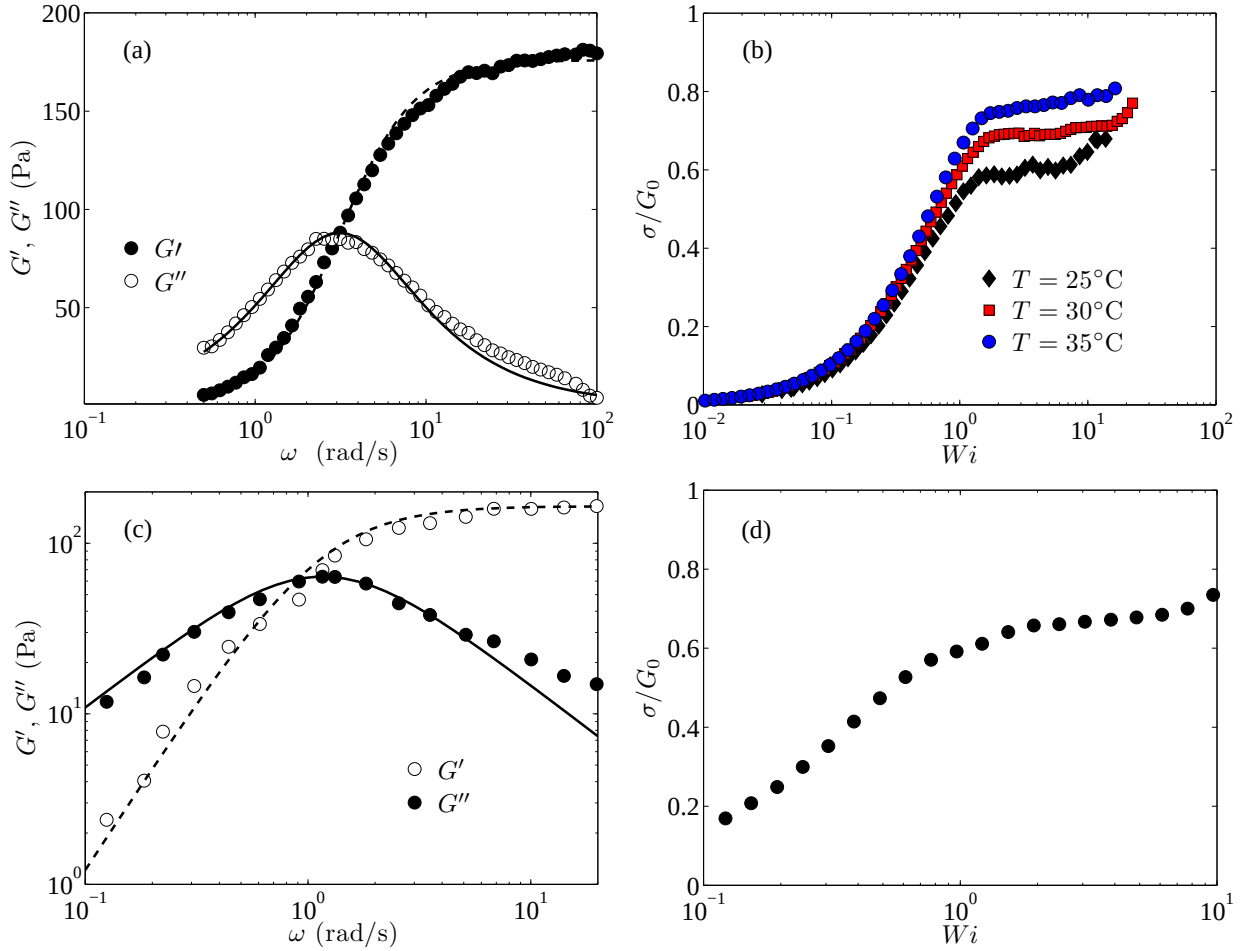

Fig. 1 (a), Elastic and loss moduli (G′,G″) measured at T = 25 C for CTAB-$NaNO_3$ (0.3M,0.4M), and (c) For CPCl-NaSal (8wt%,) at T = 21 C with the predictions of the Maxwell model (lines). (b) Normalized steady shear stress as a function of Wi measured for CTAB-$NaNO_3$, and (d) CPCl-NaSal.

= 0.5 mm, with corresponding radius ratios R_i/R_o of 0.91, 0.94, and 0.96, where d is the difference between the outer and inner radii. Flow visualization experiments were performed in a custom-built Taylor-Couette cell to visualize the interface dynamics of the wormlike micellar solution. This Taylor-Couette cell enables us to rotate both the inner and outer cylinders independently. The radii of the inner and the outer cylinders are 6.946 cm and 7.615 cm respectively, which provides a radius ratio of 0.91. The large gap allows high resolution of the interface dynamics in the r-z plane, which is imaged with a CCD camera. The height of the Taylor-Couette cell is 40.6 cm corresponding to the aspect ratio of 60.7 that renders the end effects negligible. For further information on the TC cell please see reference[44].

3 Results

3.1 Rheological Characterization

The system of wormlike micelles used in this work has been well studied by other researchers[15,21,36]. Small amplitude oscillatory shear experiments were performed in a cone-and-plate geometry to extract the relaxation time τ_R and plateau modulus G_0 of the fluid. Figures (1a) and (1c) show typical experimental results along with the predictions of the Maxwell model (equations (4) and (5)) at T = 25 C for the CTAB-$NaNO_3$ system and at T = 21 C for the CPCl-NaSal system.

$$G'(\omega) = \frac{\omega^2 {\tau_R}^2}{1+\omega^2 {\tau_R}^2} G_o \quad (4)$$

$$G''(\omega) = \frac{\omega \tau_R}{1+\omega^2 {\tau_R}^2} G_o \quad (5)$$

Where G', G'', ω, τ_R and G_0 are elastic modulus, loss modulus, frequency, relaxation time and plateau modulus respectively. The list of relaxation times and plateau moduli at different temperatures is given in table (1).

Sample	Temperature (C)	τ_R (s)	G_0 (Pa)
	25	0.32	185
CTAB-$NaNO_3$	30	0.18	200
	35	0.06	210
CPCl-NaSal(E)	21	0.87	155
CPCl-NaSal(NE)	21	0.89	152

Table 1 Relaxation times and plateau moduli for CTAB-$NaNO_3$ and CPCl-NaSal systems. E and NE denote the CPCl-NaSal samples with and without history of ambient light exposure.

We have also carried out steady shear experiments to measure the shear stress σ as a function of shear rate $\dot{\gamma}$ at different temperatures. Figures (1b) and (1d) show the dimensionless stress versus Weissenberg number for the two wormlike micellar systems. The Weissenberg number, Wi, is defined as the magnitude of the shear rate, $\dot{\gamma}$, multiplied by the Maxwellian relaxation time, τ_R. The results at different temperatures collapse onto each other and form a superimposed curve outside the shear banding regime. The shear banding plateau is clearly visible in figure (1b) and (1d), beginning at Wi $\approx$ 1. The results of small amplitude oscillatory shear and steady shear for these systems are in good agreement with literature results [15,21,36,39].

3.2 Dynamics of the interface between shear bands

As noted above, experiments on some wormlike micellar systems in a Taylor-Couette cell have shown that above a critical shear rate, the fluid splits into a high shear band and a low shear band, with the interface between them undergoing a series of stages [15,36]. Here, we examine the interface travel stage via: 1) direct visualization in a large Taylor-Couette cell, and 2) superposition rheology using Mooney-Couette geometries.

3.2.1 Direct visualization

Figure (2a) shows a schematic of our TC cell with a camera positioned to visualize the flow of the wormlike micelle solution in the r-z plane. For all experiments reported below we use a high speed ramp of the inner cylinder from rest to achieve the final shear rate quickly ($d\Omega/dt$ = 5 Hz/s), and observe the interface dynamics in the gap between the inner and outer cylinder walls. Figure (2b) shows images of the CTAB-$NaNO_3$ wormlike micelle solution sheared at Wi = 5.5 at T = 30 C as a function of time. Consistent with the earlier observations of Lerouge and co-workers [15,36], we identified four stages in the evolution of the interface. These are: 1) formation of a high shear phase that occupies the entire gap (t = 0.5 s), 2) interface construction as the interface between the high shear and low shear phases forms and sharpens (t = 2−7 s), 3) interface travel as the sharp interface moves to an equilibrium radial position (t = 7.5−25 s), and 4) interface undulation as the originally flat interface becomes destabilized and wavy (t = 25−60 s). These undulations are characterized by an asymptotic wavelength that can be identified in the last image in figure (2b). In this study, we are mainly concerned with the dynamics of the interface during the third stage. As noted above, the stress diffusion coefficient can be evaluated by measuring the speed at which the interface travels to its equilibrium position. Radulescu *et al.* [15] showed that the position of the interface in the small gap approximation is given by:

$$r_i - r^* = (r_0 - r^*)e^{-t/\tau} \quad (6)$$

where r_i is the radial position of the interface, r^* is the equilibrium radial position, r_0 is the initial position of the interface and t is time. The characteristic time τ is given by $\tau = \frac{\tau_R^2 dKG_0\dot{\gamma}}{\sqrt{D\tau_R}\eta_l\dot{\gamma}_l(\dot{\gamma}_h-\dot{\gamma}_l)}$, where, η_l is the viscosity of the wormlike micelle solution

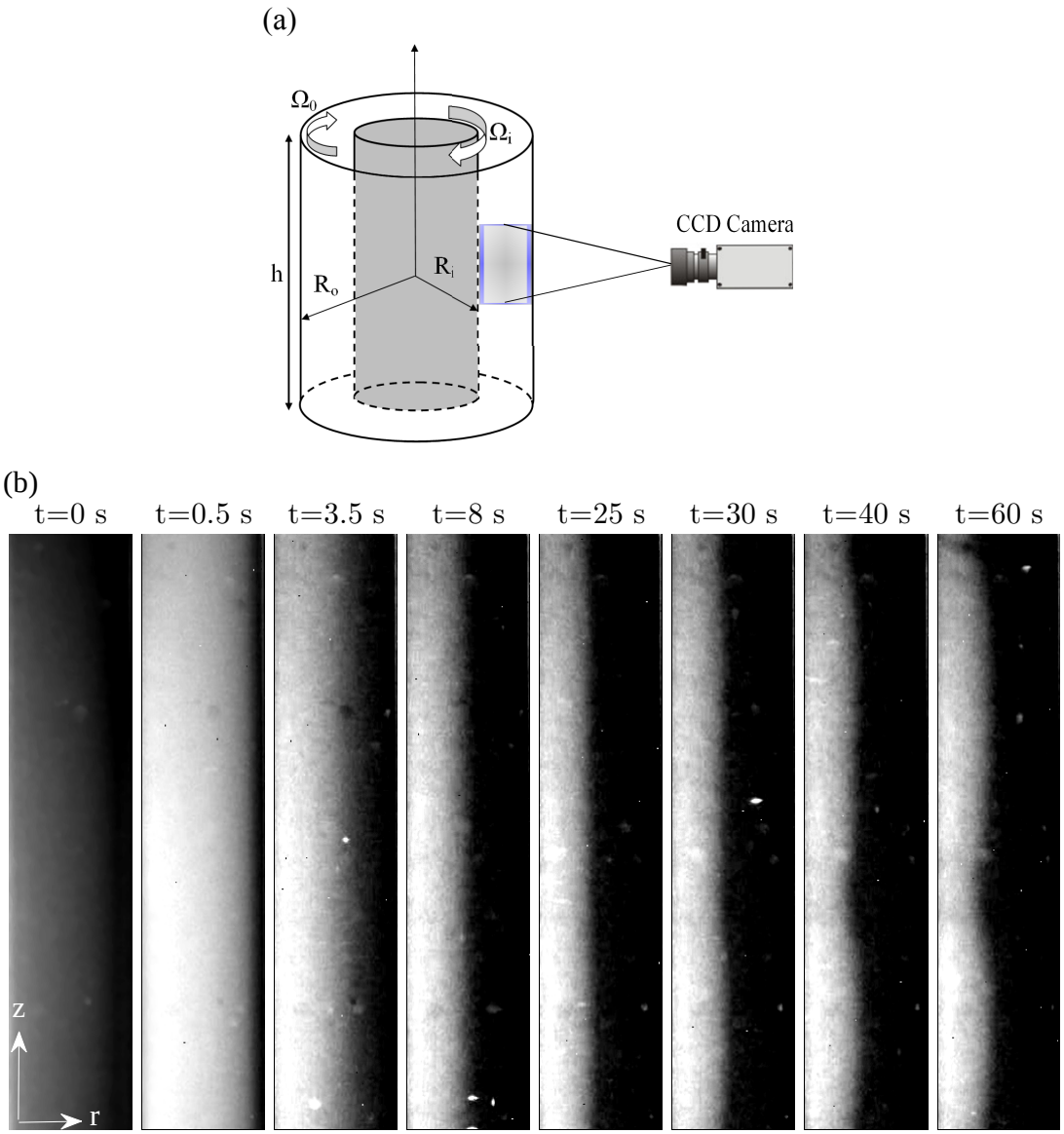

Fig. 2 (a) A schematic of the custom made Taylor-Couette cell used in experiments. (b) Images of the sheared wormlike micellar system within the shear banding regime at different times.

before shear banding and K is a dimensionless parameter that depends on the constitutive model. For the diffusive Johnson-Segalman model, Radulescu *et al.*[15] showed by scaling analysis and numerical simulations that $\frac{KG_0\tau_R}{\eta_l\dot{\gamma}_l} \approx 0.3-0.4$. Thus, once τ is determined from the interface travel, the stress diffusion coefficient and the stress correlation length can be estimated. We have tracked the interface position as a function of time by tracking the light intensity as a function of radial position within the gap. The wormlike micellar solutions are seeded with mica flakes, so that the high shear band has a much higher intensity than the low shear band. The intensity gradient between the two bands allows us to track the interface position. Sample plots showing the intensity versus radial position for various times during the interface evolution are provided in the supplementary material (see Figure S.1). We have fitted a sigmoid function ($y = \frac{a}{b + e^{-\frac{r-r_i}{w}}}$) to the experimentally determined intensity profiles

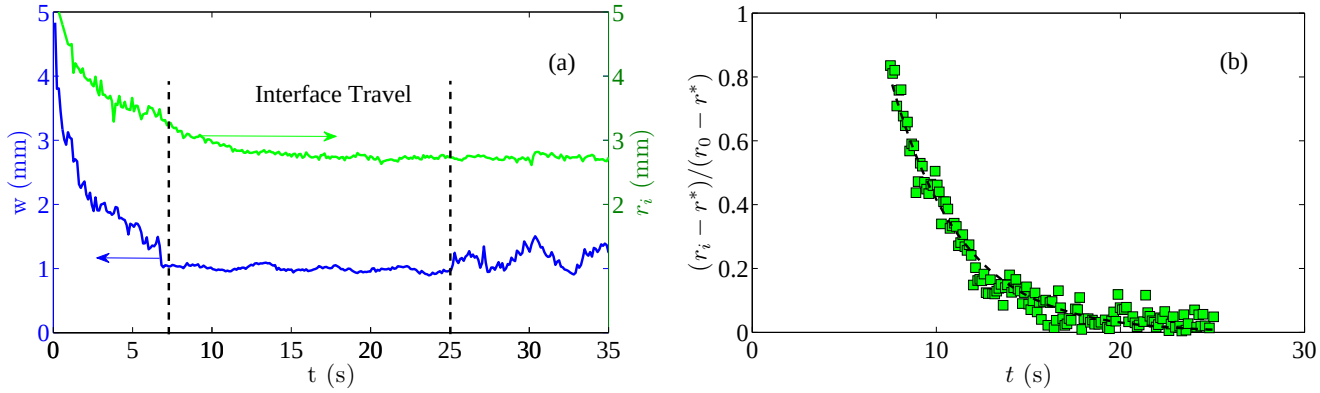

Fig. 3 (a) Interface position r_i and thickness of the interface w versus time t measured in TC cell as the external shear rate undergoes a step from 0 to 30 (1/s) at T = 30 C. (b) Interface location during the interface travel stage. The solid line is the best exponential fit to equation (6).

(black curves in figure S.1). The location of the interface is assumed to be at the inflection point of the fitted curve and is denoted as r_i. Moreover, the visible thickness of the interface between dark and bright phases is also estimated as w. Other sigmoidal functions such as the complementary error function were also considered and resulted in similar r_i and w. We further monitor the temporal evolution of these two parameters during step shear experiments. Figure 3(a) shows the temporal change in radial position r_i and thickness of the interface w. The interface travel stage is identified as the time interval when the interface width reaches and maintains its minimum value, shown between two dashed lines indicated in figure 3(a). It is evident that the visible thickness of the interface between dark and bright phases is approximately constant ($w \approx 1$ mm) during the interface travel stage, while the interface position gradually moves towards the inner cylinder. The onset of interface travel corresponds to $t_5 = 7.5\ s$ in figure (S.1). A similar plot to figure (3) for other conditions is provided in supplementary materials (cf. Figure S.2). Figure (3b) shows a typical example of interface motion during the interface travel stage up to the time when the interface starts to undulate with the best exponential fit from equation (6).

Figure (4a) shows the stress diffusion coefficient, extracted from measurements such as those shown in figure (3b), as a function of Weissenberg number at different temperatures. Our results show that the stress diffusion coefficient is approximately independent of the Weissenberg number. This trend is roughly consistent with the results presented in the literature for the CTAB-$NaNO_3$ system[43] (cf. Fig. (22d) therein) with less variation in the stress diffusion coefficient over the range of shear rates. We also note that the dependency of the stress diffusion coefficient with respect to shear rate is fully consistent with results of Masselon *et al.*[41,42] in flow of wormlike micelles in microchannels. Figure (4b) also shows the stress diffusion coefficient averaged over the range of Weissenberg numbers examined as a function of temperature. The inset of figure (4b) also indicates that $\zeta = (D\tau_R)^{1/2}$ is approximately independent of temperature in the range studied here. Although we know of no scaling laws for the stress diffusion coefficient, we note that for polymer solutions, the species diffusion coefficient follows the Stokes-Einstein equation and is proportional to temperature while the relaxation time varies inversely with temperature for a Rouse or Zimm chain, so that the product $D\tau_R$ is expected to be independent of temperature[45]. This appears, from figure (4b) (and its inset), to also be the case for the stress diffusion coefficient.

The mesh size ξ of wormlike micelles can be estimated by $\xi = (k_B T/G_0)^{1/3} \approx 32.7$ nm at T = 30 C, where, k_B is the Boltzmann constant. Our results in figure (4) gives a stress correlation length of $\zeta \approx 20\ \mu m$ indicating that $\zeta \gg \xi$, consistent with[36,41–43]. The most surprising observation is the magnitude of the stress diffusion coefficient. The average diffusion coefficient measured in our experiments at T = 30 C is about $D \approx 2.9 \times 10^{-9} m^2/s$, while those that have been reported for the same system are about $D \approx 7 \times 10^{-11} m^2/s$ and $D \approx 8.5 \times 10^{-11} m^2/s$[36,43]. This factor of 40 is striking, because the only difference between these two systems is the gap of the Couette geometry. However, the radius ratio for all these experiments is > 0.91, so that all experiments are carried out in the narrow gap limit with curvature playing a very limited role. To examine the discrepancies between our results and those in the literature, and to probe the potential role of the gap size more thoroughly, we use superposition rheology experiments in a commercial rheometer, in which a range of gap sizes could be easily accessed.

3.2.2 Superposition Rheology

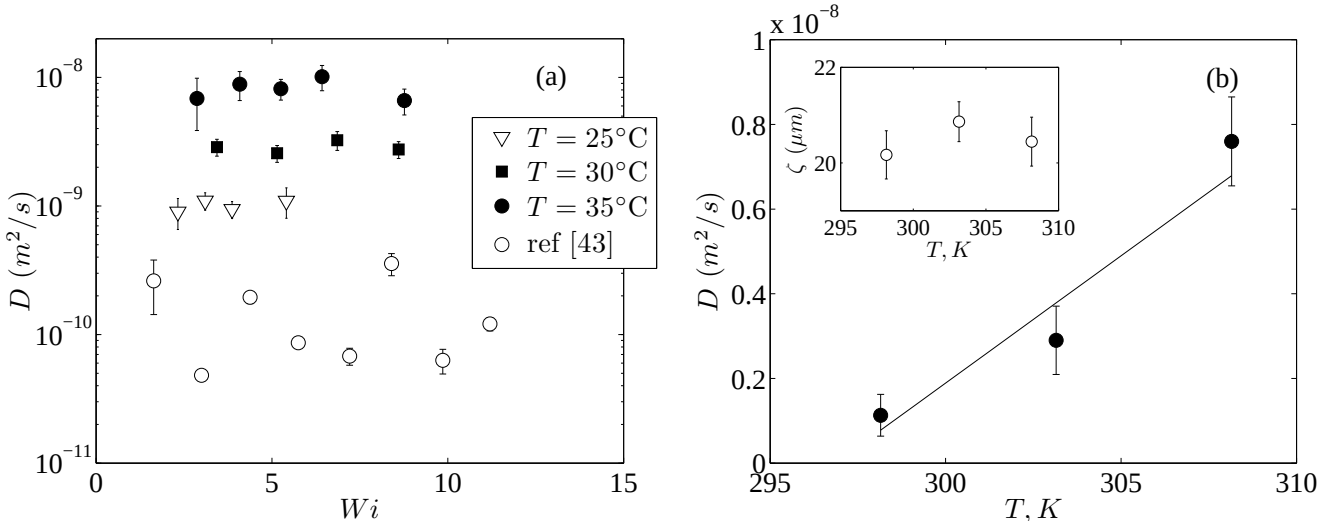

Fig. 4 (a) Stress diffusion coefficient as a function of Weissenberg number at three temperatures. These values are determined from measurements of the interface travel. (b) Stress diffusion coefficients averaged over Weissenberg number versus temperature. Inset shows the stress correlation length as a function of temperature.

Superposition rheology is an alternative method that can be utilized to determine the stress diffusion coefficient of wormlike micelles. Ballesta *et al.*[39] used this method to determine the velocity of the interface and related that to the stress diffusion coefficient during the interface travel stage for a wormlike micelle solution of cetylpyridinium chloride (CPCl) and sodium salicylate (NaSal). Here, we apply their method to the CTAB-$NaNO_3$ system described above. As shown by Ballesta *et al.*[39], for the Mooney-Couette geometry the complex viscosity from superposition rheology is given by:

$$\frac{1}{\eta^*_{\parallel}} = \frac{1-\alpha}{\eta^*_{\parallel l}} + \frac{\alpha}{\eta^*_{\parallel h}} + \frac{\dot{\gamma}_h - \dot{\gamma}_l}{\sigma_c}\frac{c_0}{i\omega d}\left(\frac{\varepsilon_{co}}{1-\frac{2ic_0}{\omega R_i}} + 2\varepsilon_{cp}\right) \tag{7}$$

Where $\eta^*_{\parallel}$, $\eta^*_{\parallel l}$, $\eta^*_{\parallel h}$, α, c_0, σ_c, and ω are the complex viscosity of the fluid from superposition rheology, the complex viscosity of the fluid at the onset of shear banding (i.e., in the limit that the fluid is completely isotropic), the complex viscosity of the fluid at the end of shear banding, the proportion of shear induced structure due to the steady shear, the velocity of the interface, the critical stress for the onset of shear banding, and the frequency of the imposed oscillation respectively. α can be calculated from the lever rule:

$$\dot{\gamma} = \alpha\dot{\gamma}_h + (1-\alpha)\dot{\gamma}_l \tag{8}$$

Where $\dot{\gamma}$ is the imposed steady shear rate. Meanwhile, ε_{co} and ε_{cp} are the proportions of the surface covered by Couette and cone-and-plate geometries, respectively. These can be calculated using the following equations:

$$\varepsilon_{co} = \left(1+\frac{R_i}{2h}\right)^{-1},\ \varepsilon_{cp} = 1-\varepsilon_{co} \tag{9}$$

Where, R_i and h are the radius of the inner cylinder and the height of the Mooney-Couette geometry. Figure (5) shows the magnitudes of the complex viscosities measured for the wormlike micellar system studied in this work at different Weissenberg numbers. Below the onset of shear banding (Wi = 0.8), the complex viscosity is approximately constant at low frequencies ($\omega \leq 10$ rad/s) and decreases with increasing frequencies above 10 rad/s.

Increasing the Weissenberg number towards the onset of shear banding results in a deviation from the low frequency plateau. This deviation increases with increasing shear rate, which is consistent with the results of Ballesta *et al.*[39]. This indicates that the system is in the shear banding regime where the two-fluid model is needed. As noted above, we are going to use equation (7) to obtain the stress diffusion coefficient. To do so, we need c_0, the velocity of the interface during interface travel. In equation (7), all parameters can be measured in experiments, except $\eta^*_{\parallel h}$. Following Ballesta *et al.*[39], and considering the onset of shear banding ($\alpha \longrightarrow 0$), one finds:

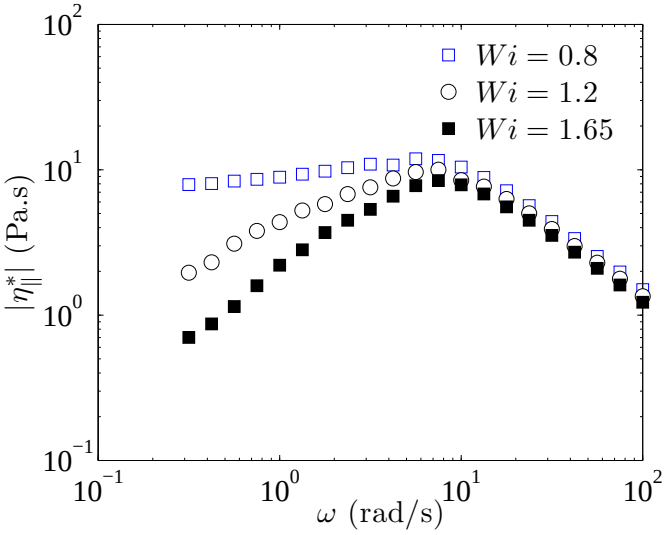

Fig. 5 $|\eta^*_{\|}|$ versus frequency for different applied Weissenberg numbers. Results are measured for CTAB-$NaNO_3$ (0.3M, 0.4M) at T = 30 C and a gap of 1.25 mm.

$$\tilde{\eta}(\omega) = \frac{\sigma_c}{\dot{\gamma}_h - \dot{\gamma}_l} \frac{i\omega d}{c_0} \left(\frac{\varepsilon_{co}}{1 - \frac{2ic_0}{\omega R_i}} + 2\varepsilon_{cp}\right)^{-1} \tag{10}$$

Where, $1/\tilde{\eta}(\omega) = 1/\eta^*_{\|}(\alpha \to 0) - 1/\eta^*_{\|_l}$. Calculating the imaginary and real parts of $\tilde{\eta}(\omega)$, we find a range of frequencies for which the imaginary part of the viscosity is higher than the real part ($\Im(\tilde{\eta}) \gg \Re(\tilde{\eta})$) (cf. Fig. 6).

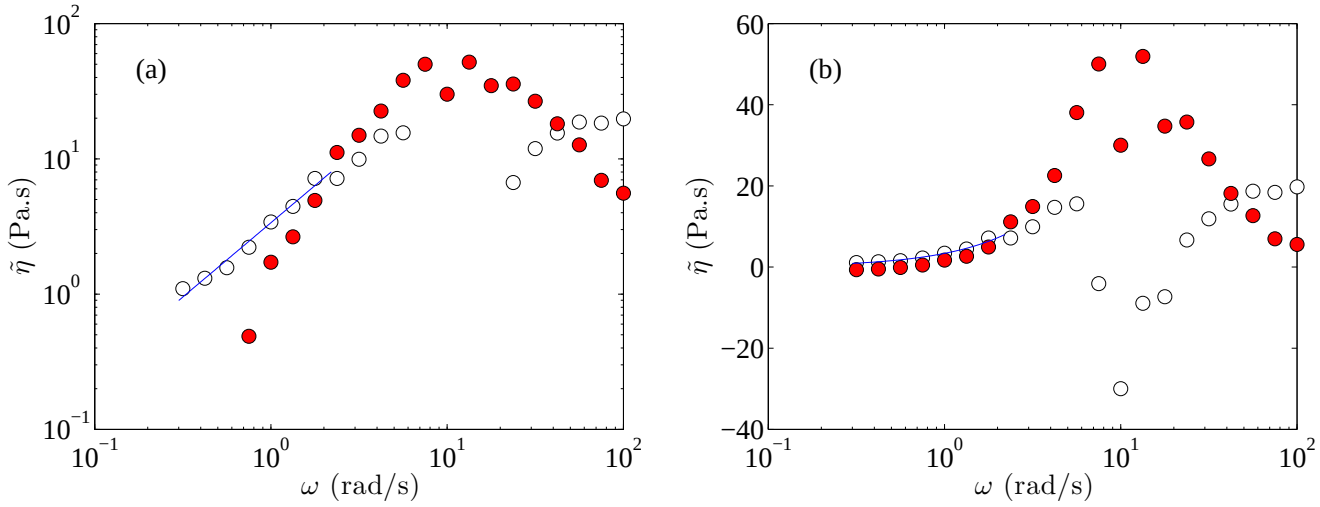

Fig. 6 (a) $\Im(\tilde{\eta})(\circ)$, $\Re(\tilde{\eta})(\bullet)$ versus frequency on log-log coordinates and (b) semi-log coordinates. Line shows the best linear fit for $0.3 < \omega < 2$ rad/s.

Therefore, similar to Ballesta *et al.*[39] we can assume that for this range of frequencies:

$$\Im(\tilde{\eta}) \approx \frac{\sigma_c}{\dot{\gamma}_h - \dot{\gamma}_l} \frac{\omega\, d}{c_0} \frac{1}{1 + \varepsilon_{cp}} \tag{11}$$

Similar plots to figure (6) for other conditions are provided in supplementary materials (cf. Figure S.3). We now can extract the velocity of the interface by fitting a linear function to the imaginary part of the viscosity. This velocity can be substituted into equation (12) to obtain the stress diffusion coefficient,

$$D = \tau_R (K G_0 c_0 / \sigma_c)^2 \tag{12}$$

Where $KG_0/\eta^*_{\|}(0,\dot{\gamma}_l)\dot{\gamma}_l = 0.3$. Figure (7) shows the diffusion coefficient resulting from the superposition rheology method as a function of temperature. The stress diffusion coefficient increases with increasing temperature in agreement with the interface travel method. The inset of figure (7) also indicates that the stress correlation length is independent of temperature in agreement with the results of interface travel.

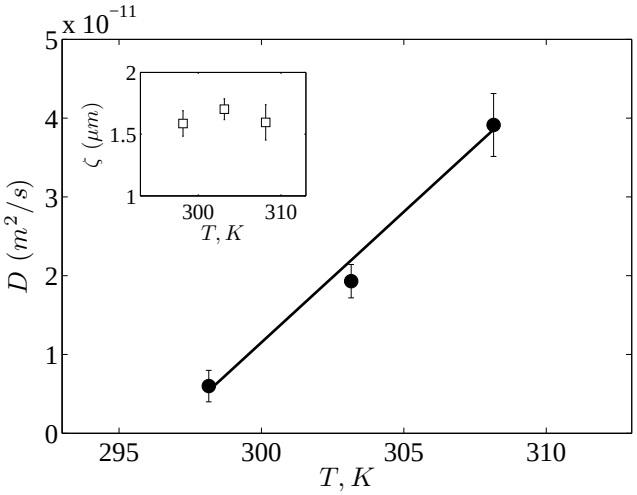

Fig. 7 Stress diffusion coefficient versus temperature for the CTAB-$NaNO_3$ system. Inset shows the stress correlation length corresponding to the diffusion coefficients.

The estimated diffusion coefficient, and the corresponding stress correlation length for a gap of 1.25 mm and T = 30 C, calculated by this method, are $D \approx 1.9 \times 10^{-11}\ m^2/s$, and $\zeta \approx 1.84\ \mu m$. These parameters are close to measurements by Lerouge and co-workers[36,43]. This suggests that this method is a promising alternative to measuring the stress diffusion coefficient and correlation length. Once again, however, if we compare the magnitude of the stress diffusion coefficient with the one reported from the interface travel method, there is a big difference and the only significant difference between these measurements is the gap of the Couette geometry. Therefore, we conducted superposition rheology measurements for a range of gap sizes.

Figure (8) summarizes the stress diffusion coefficients obtained by different methods for the CTAB-$NaNO_3$ system as a function of gap size at different temperatures. The stress diffusion coefficient increases monotonically with the gap size, with D going roughly as d^3. The inset of figure (8) also shows that the stress correlation length approximately scales as $d^{1.5}$. We also include the two available measurements for the same system reported in the literature, which are roughly consistent with this dependence and help illuminate the discrepancies. The diffusion coefficients from the interface travel method, which appear to be independent of shear rate, are averaged over all shear rates at a given temperature (cf. Figure 4(a)).

To further examine the effect of gap size on the stress diffusion coefficient, we conducted superposition rheology experiments on the well studied sample of wormlike micelles of CPCl-NaSal in brine[10,39]. We used the superposition rheology method to measure the diffusion coefficient in this system by varying the gap of the Couette geometry. Figure (9) shows the stress diffusion coefficient versus the gap of the Couette cell for the CPCl-NaSal wormlike micellar system at 21 C. Figure (9) shows that the stress diffusion coefficient for this CPCl-NaSal system also varies with gap size d as d^3, and that the measurements of Ballesta *et al.*[39] and Fardin & Lerouge[43] are consistent with this scaling. Also included in figure (9) are data on samples with no light exposure and with light exposure. We exposed one of the CPCl-NaSal samples to ambient light for one week, which resulted in a visual change in the sample from fully transparent to yellow, consistent with previous reports[22]. We note that the stress diffusion coefficient, like the bulk rheological properties, appears insensitive to light exposure.

We note that all of these experiments were performed for very narrow gaps ($0.91 < R_i/R_o < 0.96$), therefore, the effect of curvature varies negligibly between experiments. The diffusion coefficient in the dJS model can be thought of as a stress

relaxation by diffusion of differently strained wormlike chains in different shear bands[28]. According to the dJS model the thickness of the interface between different bands should scale as $\zeta = (D\tau_R)^{1/2}$. This value for the case of the large Taylor-Couette cell (where D is largest) is calculated from our experimental value of D to be of order 20 μm, hence, the interface thickness should be negligible compared to the gap size of the Taylor-Couette cell. However, our interface visualization results suggest otherwise. The visible thickness of the interface between the bright and dark phases is measured in our experiments as mentioned in section (3.2.1). Our results indicate that the thickness of the interface for all conditions is approximately $w \approx 1 \pm 0.1$ mm. Therefore, it is comparable to the gap of our Taylor-Couette cell ($\frac{w}{d} = 0.143$). Similarly, Britton *et al.*[46–48], for a CPCl-NaSal solution in Couette flow, reported a thick interface between two shear bands at high shear rates. This implies that wall effects might play a role in determining the stress diffusion coefficient during the interface travel stage.

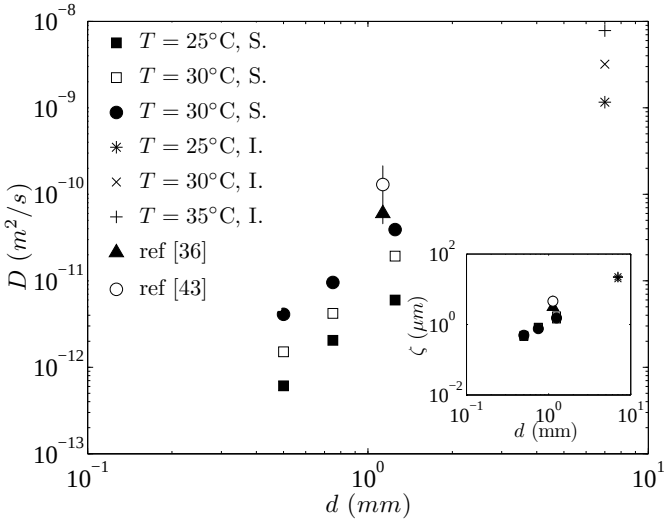

Fig. 8 Diffusion coefficient versus gap size by Superposition Rheology (S.), and Interface visualization (I.), including those reported for this (CTAB-$NaNO_3$) (0.3M,0.4M) system in the literature[36,43]. The best fit line gives the relationships $D \sim d^{2.9}$, $\zeta \sim d^{1.45}$.

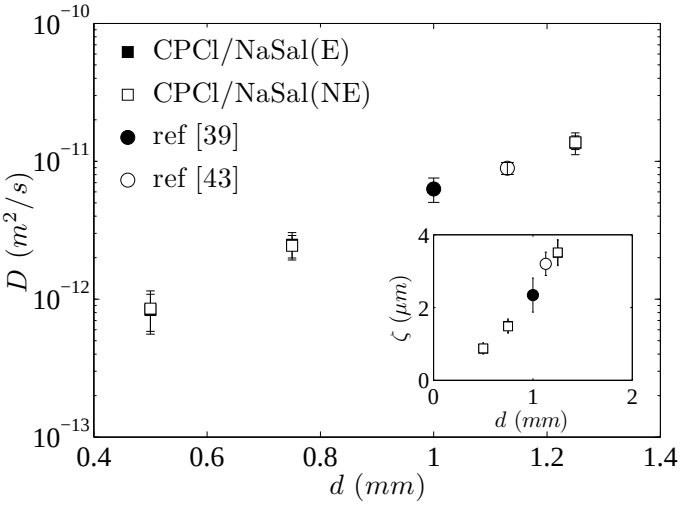

Fig. 9 Stress diffusion coefficient versus gap size measured for CPCl-NaSal from superposition rheology. Inset shows the corresponding stress correlation length versus gap size. Data for the samples with and without light exposure overlay one another. Here, the best fit to the data is $D \sim d^{3.05}$, $\zeta \sim d^{1.5}$.

We also note that slippage at the boundaries might, in principle, affect measurements of the stress diffusion coefficient. Recently, the effect of slip on the flow of different wormlike micelle systems has been investigated by measuring the local velocity profiles at different radial positions. Salmon *et al.*[17] and Hu & Lips[49], showed that slip is negligible in Mooney-Couette geometries for semidilute wormlike micellar systems of CPCl-NaSal, while Lettinga & Manneville[50] have shown, for the same system that slip results in about 40% difference between the wall velocity and the velocity of the adjacent layer of fluid and also shifts the shear banding regime by 3.4 s^{-1}. Fardin & Lerouge[43] have reported slip for the CTAB-$NaNO_3$ system. However, the slip velocity was found to be only 40% of the velocity at the rotating wall, indicating that slip is comparable for the CTAB-$NaNO_3$ and for the CPCl-NaSal systems. In superposition rheology, equation (11) and (12) show that the stress diffusion coefficient scales as: $D \sim (\frac{\eta^*_l \dot{\gamma}_l}{\dot{\gamma}_h - \dot{\gamma}_l})^2$. Therefore, we might expect slippage to affect the stress diffusion coefficient in wormlike micelles. However, slip is unlikely to affect the dynamics of the interface for the shear rates tested in this work. In our measurements, we observe little difference between the flow curves of CPCl-NaSal and CTAB-$NaNO_3$ taken at different gap sizes (see figure S.4 in supplementary materials for the data for the CPCl-NaSal system). That is, we see only nominal shifting of the shear-banding regimes for the different gap sizes, so values of $\dot{\gamma}_l$ and $\dot{\gamma}_h$ and the stress at the onset of shear banding that go into our calculation of the stress diffusion coefficient show negligible changes with gap size. This suggests that even if slip is present in our experiments with wormlike micellar systems, the magnitude of slip at the moving boundary is essentially the same for different gap sizes. Therefore, we surmise that the measured diffusion coefficient and its trend with respect to the gap size is unlikely to be affected by slip at the boundaries.

4 Conclusions

In this paper, we have studied the dynamics of the interface that forms between the shear bands of two wormlike micelle systems of CTAB-$NaNO_3$ (0.3 M, 0.4 M) and CPCl-NaSal (8%wt) in brine in narrow gap Couette devices. In particular, interface dynamics were investigated during the interface migration process. The experiments were performed in geometries of different length scales for which inertia remained negligible and curvature was nearly constant. The main findings of the work can be summarized as follows.

The stress diffusion coefficient and the stress correlation length were calculated for the interface travel stage after a step shear using two methods including direct visualization and superposition rheology. The diffusion coefficient for the CTAB-$NaNO_3$ system is approximately proportional to the temperature and is independent of the shear rate. The latter observations with respect to the shear rate dependence are consistent with observations reported in the literature; these appear to be the first data regarding the temperature dependence of D for this system. Our measurement of the stress correlation length in a geometry with a gap of 1.25 mm is consistent with that of Lerouge and co-workers for the CTAB system using a gap of 1.13 mm, and with those of Ballesta *et al.* for the CPCl-NaSal system performed in a geometry with a gap of 1 mm[36,39,43]. However, the stress diffusion coefficients of both these systems monotonically increase with the gap size d, and follow a scaling of $D \sim d^3$. This trend is consistent with data reported here and by others that spans a factor of 30 in gap and almost five orders of magnitude in D. We also note that the exposure of the CPCl-NaSal system to ambient light does not change the stress diffusion coefficient. We can think of two possible causes for the effect of gap size on the stress diffusion coefficient: First, this dependency might be due to the finite thickness of the interface compared to the gap size, as has been suggested for other semidilute wormlike micellar fluids[46–48]. Our visualization of the interface between the bright and dark phases also indicates a relatively thick interface ($\sim$ 14% of the gap thickness), suggesting that the presence of the walls may be affecting the measurement of D. Second, it is possible that the growth of the interface instability begins close to the onset of the step in shear rate, and affects the interface travel stage. The time scales associated with these processes may then be affected by the gap, which controls the wavelength of the instability. Experiments to assess either of these possibilities are beyond the scope of the present work. The explanation for the variation of the stress diffusion coefficient for the CTAB-$NaNO_3$ and CPCl-NaSal systems with the gap size still remains unclear. The experimental results of this paper thus present a new challenge for theorists and those engaged in simulations using the diffusive Johnson-Segalman model in the future.

5 Acknowledgements

We gratefully acknowledge the financial support of this work by ACS PRF and the National Science Foundation through Award CBET 1335653.

References

1 R. G. Larson, *The Structure and Rheology of Complex fluids*, Oxford University Press, New York, 1999.
2 P. Coussot, J. S. Raynaud, F. Bertrand, P. Moucheront, J. P. Guilbaud, H. T. Huynh, S. Jarny and D. Lesueur, *Phys. Rev. Lett.*, 2002, **88**, 218301.
3 J. Sprakel, E. Spruijt, M. A. Cohen Stuart, N. A. M. Besseling, M. P. Lettinga and J. van der Gucht, *Soft Matter*, 2008, **4**, 16961705.
4 L. Becu, S. Manneville and A. Colin, *Phys. Rev. Lett.*, 2006, **96**, 138302.
5 W. Losert, L. Bocquet, T. C. Lubensky and J. P. Gollub, *Phys. Rev. Lett.*, 2000, **85**, 1428–1431.
6 J. F. Berret, *Equilibrium Properties and Shear-banding Transition, in Molecular Gels*, Springer, Dordrecht, 2005.
7 M. E. Cates and S. Fielding, *Advances In Physics*, 2006, **55(7-8)**, 799–879.
8 S. Lerouge and J.-F. Berret, in *Shear-Induced Transitions and Instabilities in Surfactant Wormlike Micelles*, Springer, Berlin/Heidelberg, 2010.
9 J.-F. Berret, G. Porte and J.-P. Decruppe, *Phys. Rev. E*, 1997, **55**, 1668–1676.
10 H. Rehage and H. Hoffmann, *Mol. Phys.*, 1991, **74**, 933.
11 E. Wheeler, P. Izu and G. G. Fuller, *Rheol Acta*, 1996, **35**, 139–149.
12 C. A. Dreiss, *Soft Matter*, 2007, **3**, 956–970.
13 M. E. Cates, *J. Phys. Chem.*, 1990, **94(1)**, 371–375.
14 S. Lerouge, J. P. Decruppe and P. Olmsted, *Langmuir*, 2004, **20**, 11355–11365.
15 O. Radulescu, P. D. Olmsted, J. Decruppe, S. Lerouge, J. F. Berret and G. Porte, *Europhys. Lett.*, 2003, **62**, 230.
16 J. Decruppe, E. Cappelaere and R. Cressely, *J. Phys. II*, 1997, **7**, 257–270.
17 J. B. Salmon, A. Colin, S. Manneville and F. Molino, *Phys. Rev. Lett.*, 2003, **90**, 228303.
18 M. R. Lopez-Gonzalez, M. R. Holmes, P. T. Callaghan and P. J. Photinos, *Phys. Rev. Lett.*, 2004, **93**, 268302.
19 W. M. Holmes, M. R. Lopez-Gonzales and P. T. Callaghan, *Europhys. Lett.*, 2003, **64**, 274.
20 M. E. Cates, *Macromolecules*, 1987, **20**, 2289–2296.
21 M. A. Fardin, T. J. Ober, V. Grenard, T. Divoux, S. Manneville, G. H. McKinley and S. Lerouge, *Soft Matter*, 2012, **8**, 10072–10089.
22 M. A. Fardin, T. Divoux, M. A. Guedeau-Boudeville, I. Buchet-Maulien, J. Browaeys, G. H. McKinley, S. Manneville and S. Lerouge, *Soft Matter*, 2012, 2535–2553.
23 J.-F. Berret, *Molecular Gels.*, Springer, Netherland, 2006.
24 M. Johnson and D. Segalman, *J. Non-Newton. Fluid. Mech.*, 1977, **2**, 255–270.
25 S. M. Fielding, *Soft Matter*, 2007, **3**, 1262–1279.
26 S. M. Fielding and P. D. Olmsted, *Phys. Rev. Lett*, 2006, **96(10)**, 4.
27 S. M. Fielding, *Phys. Rev. Lett.*, 2010, **104**, 198303.
28 P. D. Olmsted, O. Radulescu and C.-Y. D. Lu, *J. Rheol.*, 2000, **44**, 257.
29 D. S. Malkus, J. S. Nohel and B. J. Plohr, *SIAM (Soc. Ind. Appl. Math) J. Appl. Math.*, 1991, **51**, year.
30 G. C. Georgioua and D. Vlassopoulosb, *J. Non-Newton. Fluid. Mech*, 1998, **75**, 899–929.
31 M. M. Fyrillasa, G. C. Georgioua and D. Vlassopoulosb, *J. Non-Newton. Fluid. Mech*, 1999, **82**, 105–123.
32 J. F. Berret, D. C. Roux and G. Porte, *J Phys II (France)*, 1994a, **4**, 12611279.
33 P. Boltenhagen, Y. T. Hu, E. F. Matthys and D. J. Pine, *Phys. Rev. Lett*, 1997, **79**, 2359–2362.
34 P. T. Callaghan, M. E. Cates, C. J. Rofe and J. A. F. Smeulders, *J. Phys. II*, 1996, **6**, 375–393.
35 C. Grand, J. Arrault and M. E. Cates, *J Phys II*, 1997, **7**, 1071–1086.
36 S. Lerouge, M. A. Fardin, M. Argentina, G. Gregoire and O. Cardoso, *Soft Matter*, 2008, **4**, 1808–1819.
37 M. A. Fardin, D. Lopez, J. Croso, G. Grégoire, O. Cardoso, G. H. McKinley and S. Lerouge, *Phys. Rev. Lett.*, 2010, **104**, 178303.
38 S. Lerouge, M. Argentina and J. P. Decruppe, *Phys. Rev. Lett.*, 2006, **96**, 088301.
39 P. Ballesta, M. P. Lettinga and S. Manneville, *J. Rheol.*, 2007, **51**, 1047.
40 C. H. Booij, *Rheologica Acta*, 1966, **5**, 222–227.
41 C. Masselon, J.-B. Salmon and A. Colin, *Phys. Rev. Lett.*, 2008, **100**, 038301.
42 C. Masselon, A. Colin and P. D. Olmsted, *Phys. Rev. E*, 2010, **81**, 021502.
43 M. Fardin and S. Lerouge, *Eur. Phys. J. E*, 2012, **35**, 91.
44 C. S. Dutcher, *Ph.D. thesis, University of California, Berkeley.*, 2009.
45 R. G. Larson, *Constitutive Equations for Polymer Melts and Solutions.*, Butterworths, Boston, USA, 1988.
46 M. M. Britton and P. T. Callaghan, *Phys. Rev. Lett*, 1997, **78**, 4930–4933.
47 M. M. Britton, R. W. Mair, R. K. Lambert and P. T. Callaghan, *J Rheol*, 1999, **43**, 897–909.
48 M. M. Britton and P. T. Callaghan, *Eur Phys J B*, 1999, **7**, 237–249.
49 Y. T. Hu and A. Lips, *J. Rheol.*, 2005, **49**, 1001–1027.
50 M. P. Lettinga and S. Manneville, *Phys. Rev. Lett.*, 2009, **103**, 248302.